atmosphere

MDPI

Article

Diversity and Ranking of ENSO Impacts along the Eastern Seaboard of Subtropical Southern Africa

Ross C. Blamey * and Chris J. C. Reason

Department of Oceanography, University of Cape Town, Private Bag X3, Rondebosch, Cape Town 7701, South Africa
* Correspondence: ross.blamey@uct.ac.za

Abstract: El Niño–Southern Oscillation (ENSO) is the dominant mode of interannual climate variability over southern Africa during the summer half of the year. It is widely accepted that El Niño (La Niña) core summers (December–February) are typically warmer and drier (cooler and wetter) than average over the region. Although it is recognized that the ENSO impacts are nonlinear and not all events result in the expected impact, little or no work has been carried out to systematically explore the diversity and ranking of these impacts. Here, parameter-space bubble plots involving various rainfall and temperature metrics are used to study how such impacts vary over the eastern seaboard of subtropical southern Africa to determine the ENSO events with the strongest impacts, and to identify the most anomalous ENSO cases. Comparison of neutral summers experiencing the strongest droughts/floods with ENSO impacts is also performed. These metrics are designed to be applicable to the interests of farmers and other user groups. It is found that 1987/1988 (2017/2018) was the most unusual El Niño (La Niña) and neutral 1981/1982 had a severe drought, worse than occurs during most El Niños. These unusual cases are explained in terms of regional circulation and SST anomalies. Implications of the results for seasonal forecasting and for farmers are discussed.

Keywords: south-eastern Africa; ENSO; rainfall and temperature metrics; drought; floods

Citation: Blamey, R.C.; Reason, C.J.C. Diversity and Ranking of ENSO Impacts along the Eastern Seaboard of Subtropical Southern Africa. *Atmosphere* **2023**, *14*, 1042. https://doi.org/10.3390/atmos14061042

Academic Editors: Carlos Silveira, Sandra Rafael, António Castro Ribeiro and Myriam Lopes

Received: 26 April 2023
Revised: 5 June 2023
Accepted: 13 June 2023
Published: 17 June 2023

1. Introduction

Drought and floods are an inherent component of the climate of the eastern seaboard of subtropical southern Africa. Prominent recent examples include the threat of Day Zero in the Nelson Mandela Bay (NMB) region of the Eastern Cape [1] and the devastating floods in coastal KwaZulu-Natal (KZN) during April 2022 [2]. Like most of subtropical southern Africa, this region is characterised by summer rainfall with the December–February (DJF) period typically being the wettest [3].

On interannual scales, ENSO is widely accepted as being the most important climate mode influencing the climate of subtropical southern Africa with summer being the season when ENSO projects most strongly over the region [4–6]. In simple terms, summers are generally dry and warm (wet and cool) during El Niño (La Niña) events although there are prominent exceptions such as the 1997/1998 and 2009/2010 El Niños [7–10].

While it is known that the impacts of ENSO over subtropical southern Africa can vary substantially between events, there has not been much work to systematically categorise the impacts of each event. Thus, in this study, various rainfall and temperature metrics are used to assess the magnitude of the impacts associated with each event along the eastern seaboard of subtropical southern Africa during summer (defined here as December–February; DJF). This particular region is chosen because firstly it has been less well studied than many other agriculturally important parts of southern Africa, secondly it has experienced recent extreme drought and flood events (e.g., [1,2,11]), and thirdly it represents a transition zone from a relatively dry subtropical to the more humid tropical climate found further north. As a result, commercial agriculture in the western basin of the Eastern Cape

is dominated by sheep and irrigated stone fruit whereas sugar cane and dairy farming are important in the wetter parts of KZN. There are also large areas of subsistence agriculture throughout the eastern seaboard except over most of the western basin of the Eastern Cape, which is generally too dry to support such activities. Subsistence farming areas typically grow maize and some vegetables together with cattle and goats.

2. Materials and Methods

European Centre for Medium-Range Weather Forecast's Reanalysis v5, ERA5 [12] data were used to analyse rainfall, temperature, and circulation during the various DJF seasons during the 1979–2021 period. These data are available at 0.25° horizontal resolution. NOAA Extended Reconstructed SST, version 5 (ERSSTV5) [13] data were used to examine SST. A season was considered to be El Niño (La Niña) on the basis of the ONI index exceeding 0.75 °C (−0.75 °C) for five overlapping months up to and including the DJF season in question. To better understand regional SST patterns during selected atypical ENSO events presented, the higher resolution NOAA Optimal Interpolation SST, version 2 (OISSTV2) [14] data were used.

To assess the variation in ENSO impact along the eastern seaboard of subtropical southern Africa, four domains are analysed; namely, the western drainage basin of the Eastern Cape within which the NMB (Day Zero drought threatened area) is located, the eastern drainage basin of the Eastern Cape, southern KZN (which contains the largest port of Durban as well as the area worst affected by the April 2022 floods) and the Maputaland region to its north, which includes northern KZN/eSwatini and far southern Mozambique (Figure 1).

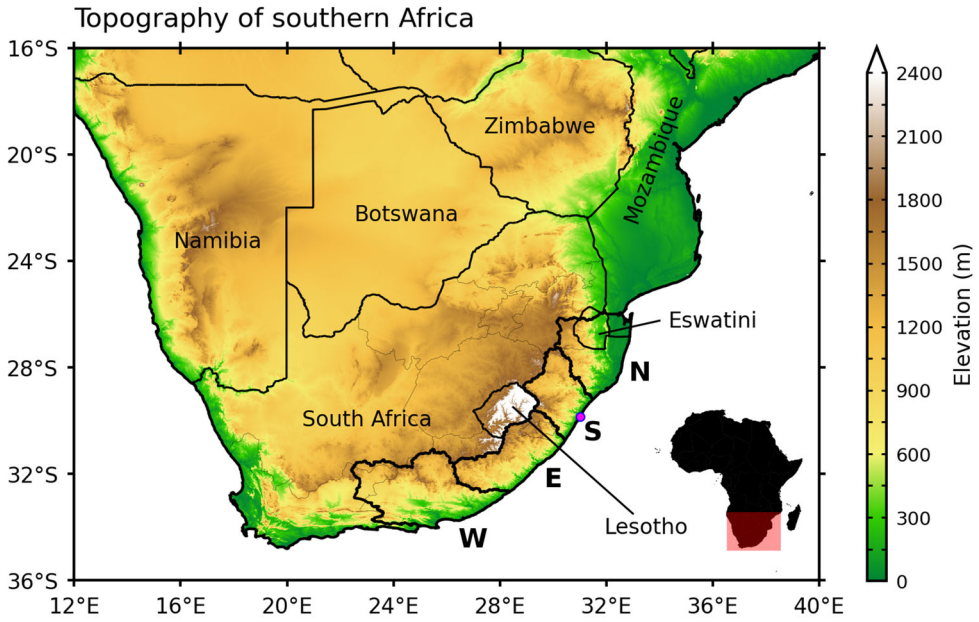

Figure 1. The topography of southern Africa (shaded; m) and the four domains used in this study. The domains are denoted by polygons labelled as W (western parts of Eastern Cape), E (eastern parts of Eastern Cape), S (southern KZN), and N (northern KZN into southern Mozambique). The small magenta circle in polygon S, along the coast, denotes the location of Durban in KZN.

The various rainfall and temperature metrics are plotted together in parameter-space with the percentage of grid cells exceeding DJF mean number of days receiving at least 10 mm of rainfall (exceeding DJF mean dry spell frequency) as the vertical (horizontal) axis. By so doing, the diversity of ENSO response in climate over the region is better revealed as well as allowing for the possibility of determining neutral summers with drought or flood characteristics similarly severe to those during the strongest-impacting ENSO events.

For each DJF season, these parameter-space bubble diagrams plot the anomaly in rainfall amount (bubble size) with the colour of each bubble representing the number of hot days. The mean DJF rainfall total is plotted as the black bubble in the bottom left-hand corner of each figure. A 'hot day' here is determined when at least 25% of the domain exceeded the grid points 90th maximum temperature percentile value. The year in the middle of the bubble is the December year of DJF (i.e., DJF 2020/2021 is indicated as 2020 on the bubble). A threshold of 10 mm rainfall was used to determine a heavy rain day based on previous analyses of rainfall distributions in the Eastern Cape and KZN [1,11]. A dry spell is determined as a pentad with at least 5 mm of rainfall as in previous studies over southern Africa [3,15,16]. The parameter-space bubble diagrams are organised into El Niño summers, neutral summers, and finally La Niña to allow easy visual comparison in a single, compact figure between extreme neutral cases and ENSO, and to see the intra-ENSO variability in rainfall metrics over each domain.

3. Results

3.1. Summer Climatology

Figure 2 shows DJF climatology of various drought-related metrics over subtropical southern Africa. There are several interesting climatological features of the eastern seaboard of subtropical southern Africa in relation to the region as a whole. Firstly, Figure 1 shows that the topographic gradient from the highest mountains in eastern Lesotho and neighbouring South Africa to the coast is particularly steep over the northern part of the Eastern Cape east basin / southern KZN and then becomes progressively less steep as one moves west along the southern escarpment from ~28° E to ~22° E. The sharp topographic gradient in the east basin / southern KZN (Figure 1) helps explain why DJF rainfall (Figure 2a) over the east basin / southern KZN as well as the number of heavy rain days (Figure 2b) is much higher than the west basin. Further north near 29° S, the escarpment is lower and moves inland, which helps explain why northern coastal KZN / southern Mozambique is generally drier with few heavy rain days than southern KZN (Figure 2a,b). Onshore flow of moist marine air across the warm Agulhas Current towards the eastern seaboard via ridging anticyclones is an important source of summer rainfall in this region [17–19] and will be enhanced where this windward flow meets steeper topography.

This difference in rain days results in mean maximum temperatures (Figure 2c) being noticeably lower over the east basin than the west and also that in southern KZN being lower than further north. While the high topography over Lesotho and the northern boundary of the east basin (Figure 1) clearly reduces maximum temperatures, the lower-lying regions near the coast of the east basin are noticeably cool relative to other coastal regions in the domain, essentially due to the relatively large number of rain days here. By the same token, dry spell frequencies in DJF (Figure 2d) are very low on average in the east basin / southern KZN but quickly increase further north up the seaboard. They also rise rapidly across the west basin of the Eastern Cape towards the Mediterranean climate of the Western Cape. Note that the two Eastern Cape basins lie on opposite sides of the southern end of the diagonal gradient in DJF dry spell frequency across subtropical southern Africa noted by authors of [3]. This gradient stands out even more clearly in the dry spell frequency–intensity map (Figure 2e), which shows less than 20% of summers during 1979–2021 to have at least half of their 18 pentads consisting of dry spells over the east basin (and eastern South Africa in general), rapidly increasing to over 80% of summers meeting that criterion over most of the west basin.

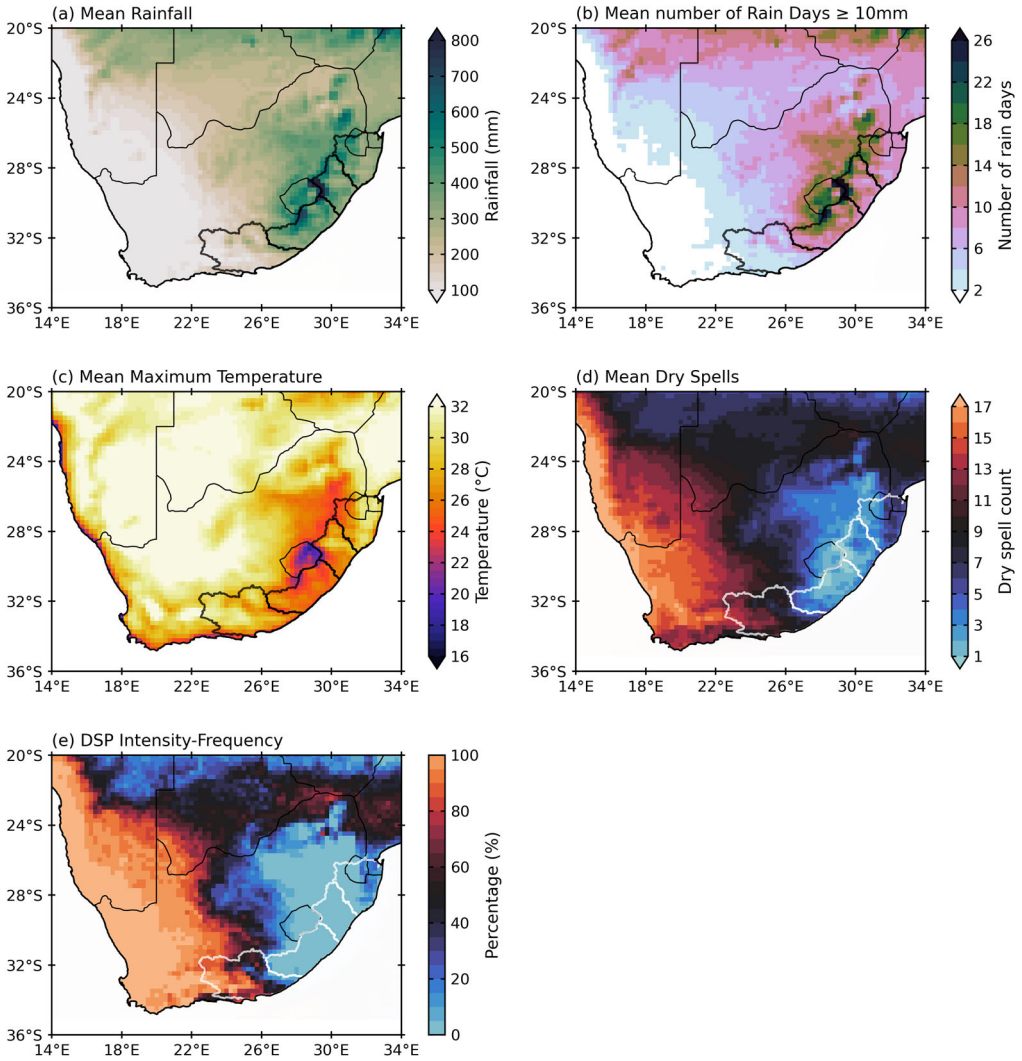

Figure 2. The December–February mean of (**a**) rainfall (mm), (**b**) number of rain days greater than or equal to 10 mm (days), (**c**) maximum temperature (°C), (**d**) dry spells (days), and (**e**) dry spell intensity–frequency (%) from the period 1979–2021. The four polygons denote the study domains.

3.2. ENSO Metric Variations

Figure 3 plots the correlation between the Niño 3.4 index and DJF rainfall over subtropical southern Africa. From this figure, it is apparent that the relationship is relatively strong over both drainage basins in the Eastern Cape (except near the coast in the western basin where it is insignificant) but weakens (although still significant) over southern KZN before strengthening again over northern KZN. The strongest relationship lies further north in Zimbabwe, northern Botswana, and southern Zambia. After spatially averaging the rainfall over each region, the Niño 3.4 index is significantly correlated at −0.53 to −0.56 with summer rainfall totals over both Eastern Cape regions and northern KZN but at only −0.36 for southern KZN (still significant at 95%). Composite DJF rainfall anomaly maps of El Niño and La Niña events suggest that generally large parts of southern Africa, stretching from the eastern seaboard up through northern South Africa into Zimbabwe and Mozambique, receive less (more) rainfall during El Niño (La Niña) (Figure A1).

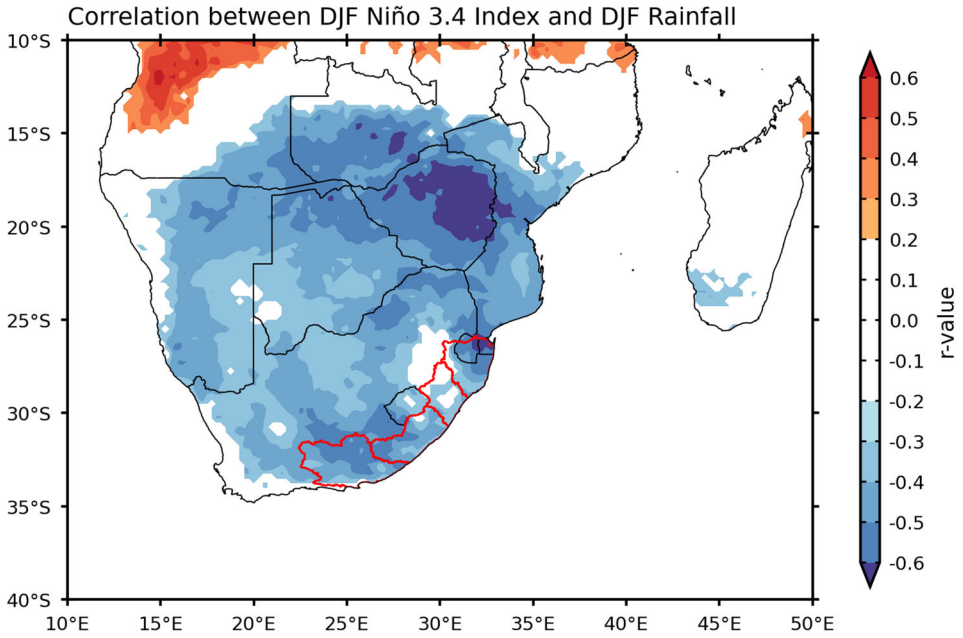

Figure 3. Pearson correlation between Niño 3.4 index and southern Africa rainfall for DJF. Only values that are significant ($p < 0.05$) are shown. The location of four domains used in the analysis are illustrated by the red polygons.

Out of nine El Niño summers, only three (1982/1983, 1991/1992, 2015/2016) fit the general expectation of falling into the lower right quadrant (small percentage of grid points experiencing above average numbers of heavy rain days and large percentage of grid points experiencing above average numbers of dry spells) with small-sized, purple-coloured bubbles (well below average rainfall and a large number of hot days) in both Eastern Cape basins (Figures 4a and 5a). For La Niña, out of 12 summers, 5 in the western basin and 3 in the eastern basin clearly fall in the upper left quadrant and have large, orange-coloured bubbles (well above average rainfall totals) and a small number of hot days (Figures 4c and 5c). The mean DJF rainfall over the western basin is only around 40% of that in the eastern basin, pointing to its much drier climate, consistent with Figure 2.

Another clear difference between the two Eastern Cape basins emerges in the neutral summers where the western basin shows a somewhat linear distribution from the upper left to the lower right quadrant (i.e., summers receiving well above average rainfall tend to have a large percentage of grid points experiencing heavy rain days and few with hot days and the reverse for the summers with below average rainfall totals) (Figures 4b and 5b). On the other hand, the eastern basin has a far wider spread of conditions across the parameter space. This difference may reflect the fact that the eastern basin is more dominated by convective rainfall, including random air mass thunderstorms, than the western basin. For organised convection, authors of [20] showed that the most important summer rainfall-producing system (tropical–extratropical cloud bands) make a greater percentage contribution to rainfall totals over the eastern than western basin in December and January (February contributions are similar). Both basins also show a few neutral summers that have similarly severe drought conditions to the most extreme El Niño summers (Figures 4a,b and 5a,b). By contrast, only the western basin has some neutral summers that have similar very wet and cooler conditions to the most extreme La Niña summers (Figures 4b,c and 5b,c). While the bubble plots allow for easy identification of the summers with the most extreme drought/flood impacts across the El Niño / La Niña spectrum, they also show obvious exceptions. For El Niño, it is apparent that 1987/1988 was the summer with the most amount of rainfall and least impact in terms of dry spells / hot days in both Eastern Cape regions (Figures 4a and 5a), whereas for La Niña, 2017/2018 was very dry and much like a severe El Niño in its impacts in both areas (Figures 4c and 5c). Since seasonal forecasting for

summer rainfall totals over South Africa only reaches useful skill for ENSO summers [21], it is important to identify the seasons where observed impacts were very anomalous.

For KZN, Figures 6a,c and 7a,c indicate that only 2 out of 9 El Niño summers clearly fall in the bottom-right quadrant in both regions whereas 4 (3) out of 12 La Niña summers obviously sit in the upper left quadrant for the southern (northern) domain. Southern KZN is wetter on average (451 mm) than the eastern basin of the Eastern Cape (413 mm) and substantially wetter than northern KZN (371 mm) on average, consistent with Figure 2. Comparison of Figures 6a and 7a with Figures 4a and 5a suggests that southern KZN domain shows the least obvious El Niño impact on heavy rain days and hot days since it has far more cases in the bottom left quadrant of the parameter space than either northern KZN or the two Eastern Cape basins. This result is reflected in the weakening of the correlation between rainfall amounts and the Niño 3.4 index (Figure 3) over southern KZN compared to the other three domains. For La Niña, southern KZN shows a concentration of summers in the upper left quadrant like the other three regions (Figures 6c and 7c). However, for the neutral summers, southern KZN (Figure 6b) is similar to the eastern basin of the Eastern Cape with a wide spread of conditions whereas northern KZN (Figure 7b) is more like the western Eastern Cape basin with a relatively linear distribution across parameter space. The strongest impacting El Niños appear to be 1982/1983 in both regions and 1991/1992 (2015/2016) for the southern (northern) domain (Figures 6a and 7a) whereas for La Niña, both domains suggest 1995/1996, 1999/2000, and 2020/2021 as having the greatest impacts (Figures 6c and 7c). In terms of exceptions, 1986/1987 (2009/2010) stand out as the least severe El Niño summers whereas 2017 (2011) appear to be the driest La Niña summers in the southern (northern) domain.

While Figures 4–7 identify 1982/1983, 2015/2016 as the worst impacting El Niño and 1999/2000 as the La Niña with the strongest impacts over the four domains, there is considerable variation in impacts for the three rainfall metrics (totals, heavy rain days, dry spells) for the other cases. As a result, the correlation between the Niño 3.4 index and rainfall totals across the eastern seaboard of South Africa while statistically significant is only moderately strong (-0.53 to -0.56 for both Eastern Cape basins and northern KZN, -0.36 for southern KZN). For the temperature metric, the ENSO response appears more consistent across the four domains with most El Niños (La Niñas) showing a large (small) number of hot days. Consistent with that result, correlations of the Niño 3.4 index with hot days are much higher over the Eastern Cape and KZN than they are for rainfall totals (~0.7 in all domains).

Based on a criterion of at least three of the four domains identifying similar values in the metrics, Figures 4–7 indicate that the 1987/1988 El Niño and 2017/2018 La Niña summers are clear exceptions to the general ENSO response over southern Africa. Similarly, 1981/1982 presents the best example of a neutral summer whose drought characteristics appear comparable to the worst El Niño impacts. These summers are investigated further in subsequent sections to see how their circulation anomalies may have contributed to the unusual impacts observed.

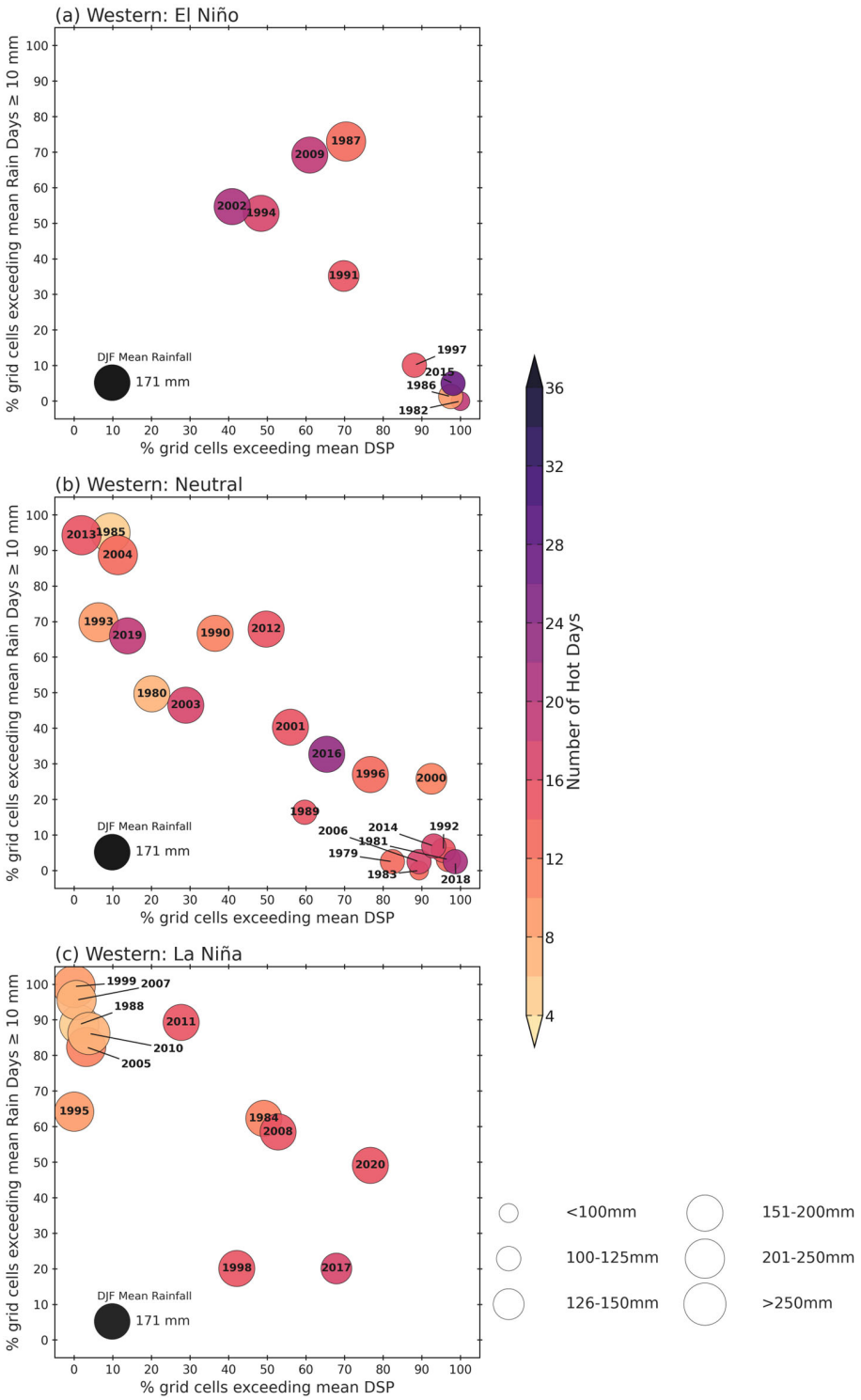

Figure 4. The bubble plots used to show the relationship between various rainfall metrics during DJF for the western basin of the Eastern Cape (see Figure 1 for location). The panels are split up as DJFs during (**a**) El Niño (**top**), (**b**) Neutral (**middle**), and (**c**) La Niña (**bottom**). Here, the y-axis shows the percentage of the grid cells that exceed the mean number of rain days $\geq$ 10 mm, while the x-axis shows the percentage of grid cells that exceed the mean dry spell count. The size of the bubble reflects the amount of rainfall for the DJF (see bubble size legend at the bottom of the panels). The mean rainfall bubble size is provided in the bottom-left corner of each panel. The colour of the bubbles reflects the number of hot days. The year in each bubble is the December of DJF (i.e., 2020 would be DJF 2020/2021).

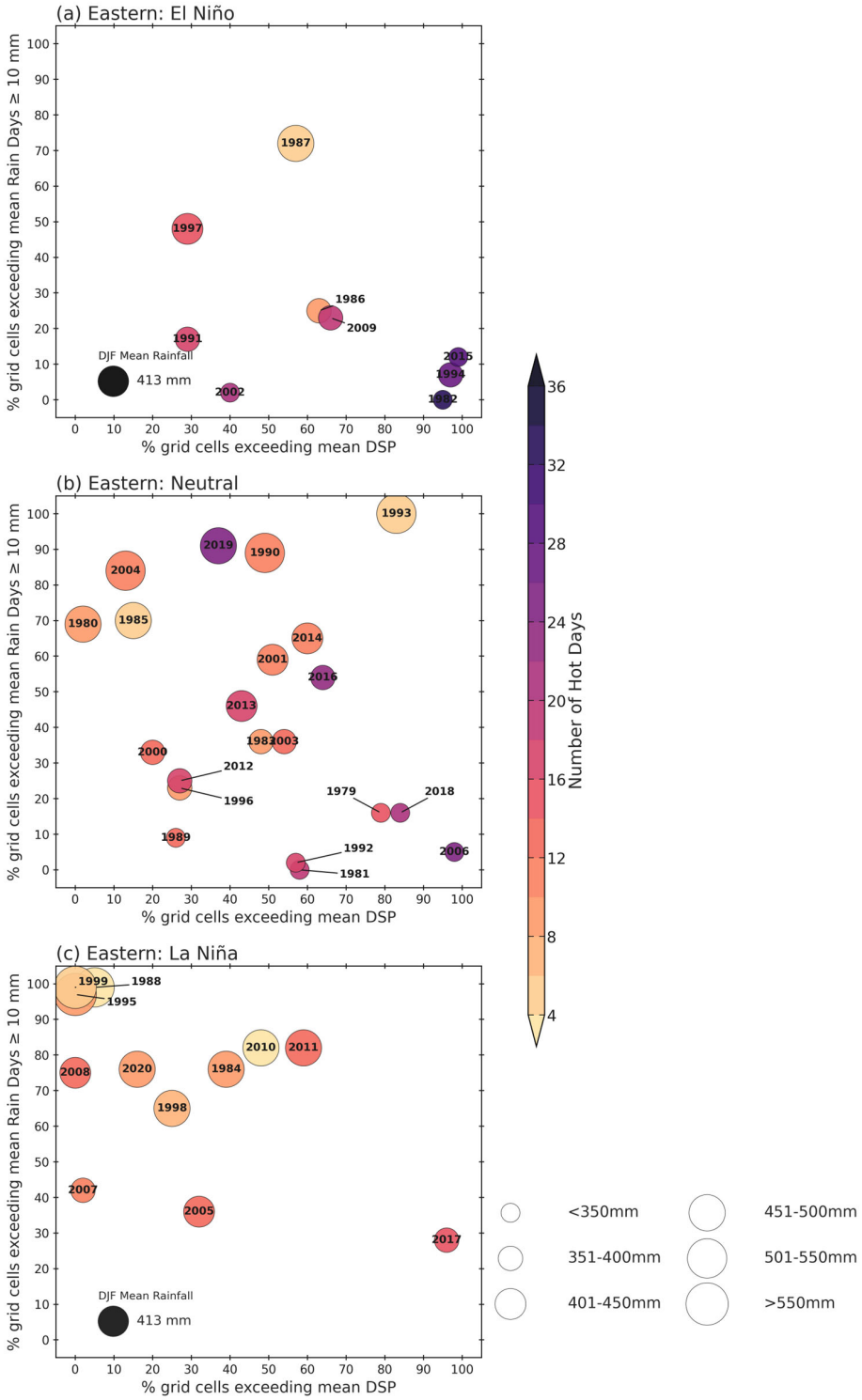

Figure 5. The bubble plots used to show the relationship between various rainfall metrics during DJF for the eastern basin of the Eastern Cape (see Figure 1 for location). The panels are split up as DJFs during (**a**) El Niño (**top**), (**b**) neutral (**middle**), and (**c**) La Niña (**bottom**). Here, the y-axis shows the percentage of the grid cells that exceed the mean number of rain days $\geq$ 10 mm, while the x-axis shows the percentage of grid cells that exceed the mean dry spell count. The size of the bubble reflects the amount of rainfall for the DJF (see bubble size legend at the bottom of the panels). The mean rainfall bubble size is provided in the bottom-left corner of each panel. The colour of the bubbles reflects the number of hot days. The year in each bubble is the December of DJF (i.e., 2020 would be DJF 2020/2021).

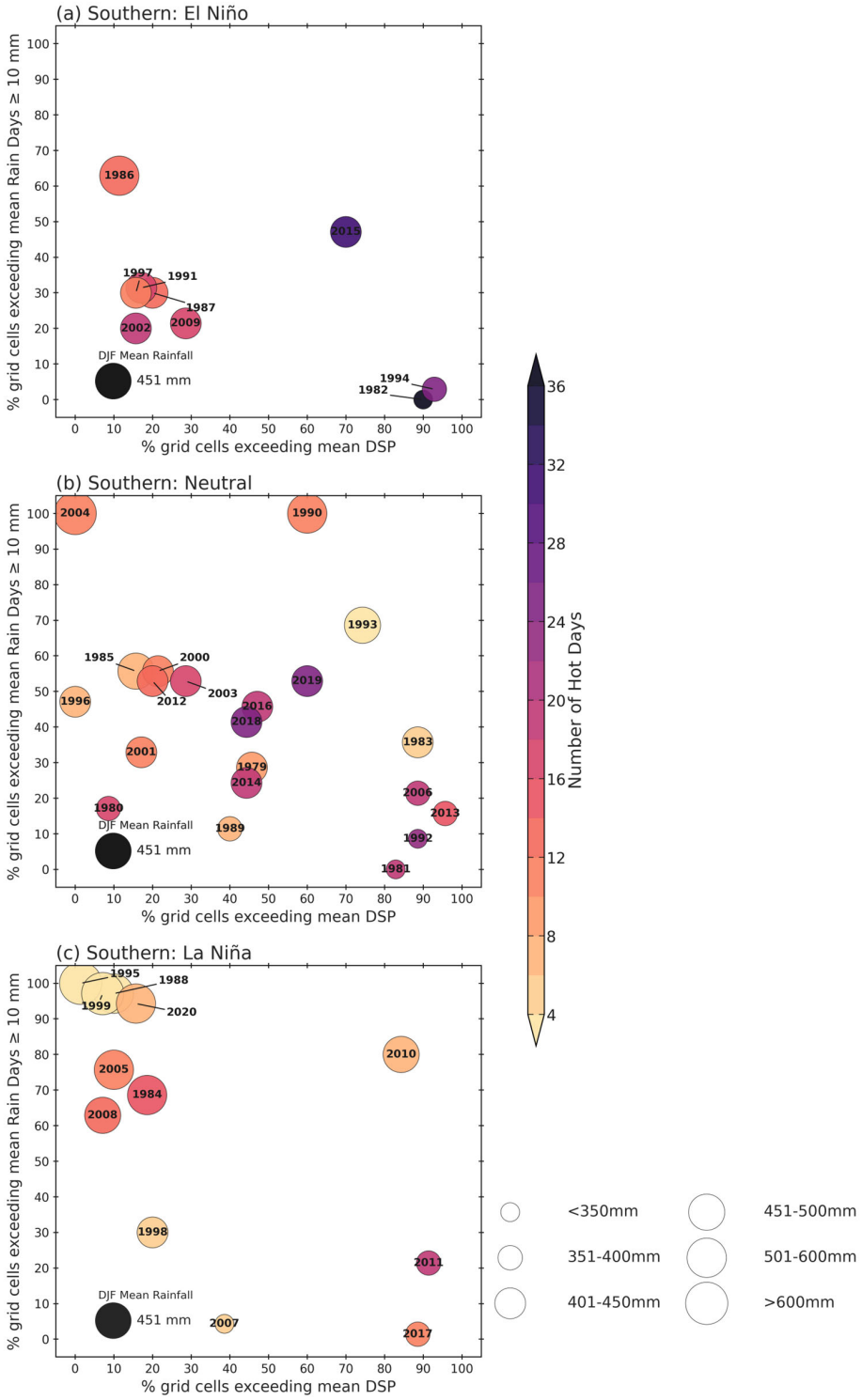

Figure 6. The bubble plots used to show the relationship between various rainfall metrics during DJF for the southern basin of the KZN (see Figure 1 for location). The panels are split up as DJFs during (**a**) El Niño (**top**), (**b**) neutral (**middle**), and (**c**) La Niña (**bottom**). Here, the y-axis shows the percentage of the grid cells that exceed the mean number of rain days $\geq$ 10 mm, while the x-axis shows the percentage of grid cells that exceed the mean dry spell count. The size of the bubble reflects the amount of rainfall for the DJF (see bubble size legend at the bottom of the panels). The mean rainfall bubble size is provided in the bottom-left corner of each panel. The colour of the bubbles reflects the number of hot days. The year in each bubble is the December of DJF (i.e., 2020 would be DJF 2020/2021).

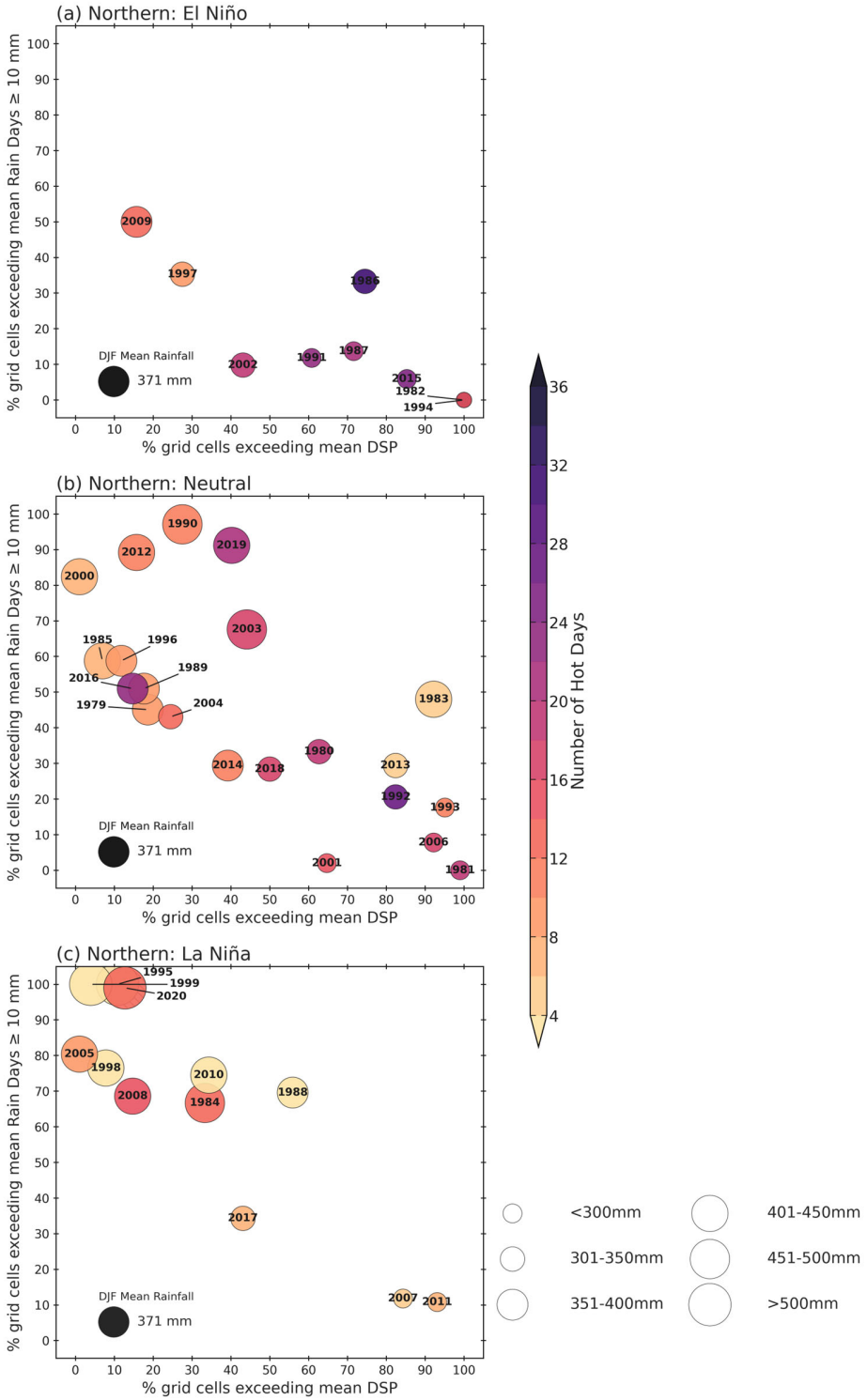

Figure 7. The bubble plots used to show the relationship between various rainfall metrics during DJF for the northern basin of the KZN (see Figure 1 for location). The panels are split up as DJFs during (**a**) El Niño (**top**), (**b**) neutral (**middle**), and (**c**) La Niña (**bottom**). Here, the y-axis shows the percentage of the grid cells that exceed the mean number of rain days $\geq$ 10 mm, while the x-axis shows the percentage of grid cells that exceed the mean dry spell count. The size of the bubble reflects the amount of rainfall for the DJF (see bubble size legend at the bottom of the panels). The mean rainfall bubble size is provided in the bottom-left corner of each panel. The colour of the bubbles reflects the number of hot days. The year in each bubble is the December of DJF (i.e., 2020 would be DJF 2020/2021).

3.3. Uncharacteristic ENSO Events

3.3.1. Anomalously Wet 1987/1988 El Niño

The 1987/1988 El Niño was a moderate event (Niño 3.4 SST anomaly in DJF of 0.8 °C) and of the central Pacific type, for which drought impacts are expected to be less severe than for the eastern Pacific types of El Niño [22]. In the South Indian Ocean, a subtropical dipole SST pattern was present, often favourable for above average rainfall over eastern South Africa [23–25] (Figure 8a). The northern Agulhas Current also displayed above average SST, favourable for wetter summers over eastern South Africa [26]. Rainfall totals were above average over the two Eastern Cape and southern KZN regions and even more so over most of central South Africa, Botswana, and Zimbabwe (Figure A2). The mechanism by which these regions received above average rainfall totals is related to increased northerly fluxes of moist marine air from the Mozambique Channel over eastern South Africa (Figure 8b) and relative uplift on the western edge of these fluxes, particularly over central South Africa and extending over most of the Eastern Cape (Figure 8d). These northerly moisture flux anomalies over eastern South Africa, Mozambique, and Zimbabwe are related to a strong anticyclonic anomaly in the southern West Indian Ocean that extends up to the 500 hPa level (Figure 8b,c). This enhanced circulation pattern then transports tropical moisture anticyclonically towards the Eastern Cape and southern KZN (Figure 8b) providing favourable conditions for increased rainfall there. Compared to the summer El Niño composite anomaly pattern [6,9], the Botswana High did not strengthen in DJF 1987/1988 unlike during more typical El Niño summers (Figure A3) when it shows large positive anomalies, and there was an anomalous anticyclonic feature over and east of southern Madagascar in 1987/1988 (Figure 8b) that is not present in the composite. This El Niño composite also has strong subsiding motion over all of southern Africa (Figure A3) unlike the band of strong uplift stretching from Botswana south-eastwards to the Eastern Cape in 1987/1988 (Figure 8d).

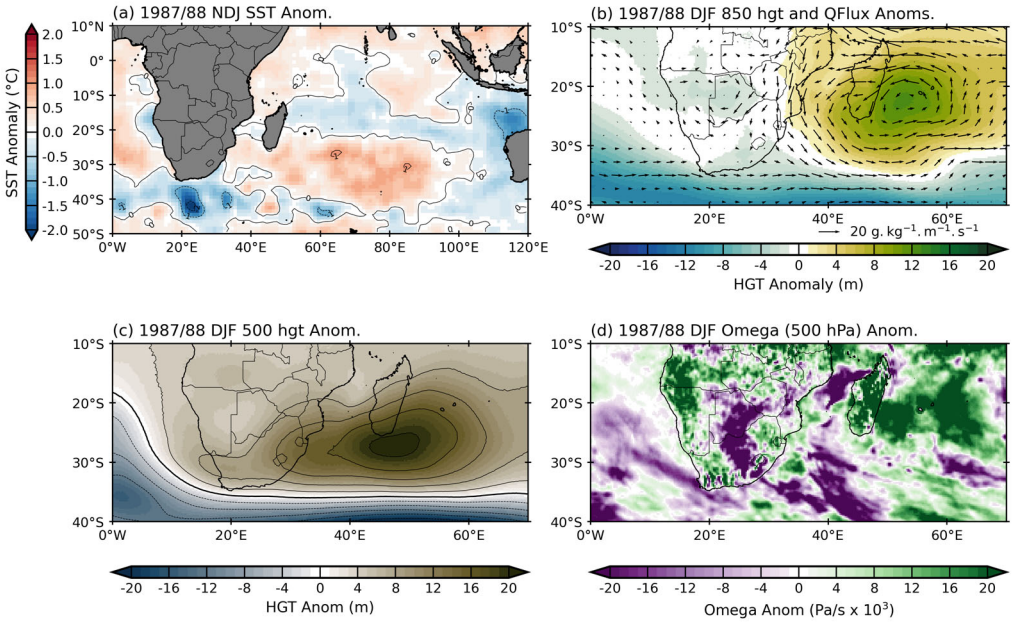

Figure 8. The 1987/1988 NDJ (**a**) SST anomalies (shaded; °C), (**b**) 850 geopotential height (shaded; m) and moisture flux (vectors; g kg^{-1} m^{-1} s^{-1}), (**c**) 500 hPa geopotential height (shaded; m), and (**d**) 500 hPa omega (shaded; Pa/s). The DJF mean (1979–2021 for ERA5 data) and NDJ mean (1981–2021 for OISST data) of variables in panels a–c are provided in Figure A4.

3.3.2. Anomalously Dry 2017/2018 La Niña

Based on the Niño 3.4 index, DJF 2017/2018 was a fairly weak La Niña summer but stronger than both 2005/2006 and 2008/2009, both of which were considerably wetter

in terms of totals than 2017/2018. Another unusual aspect about 2017/2018 is that it was an Eastern Pacific type of ENSO event which, in general, typically produce larger anomalies in summer rainfall totals over southern Africa than Central Pacific events such as 2005/2006 [22]. However, although the Pacific SST anomalies during DJF 2017/2018 were favourable for a wet summer, those in the southern West Indian Ocean were not (Figure 9a). Previous observational and modelling results have shown that negative SST anomalies here are typically associated with dry summers over eastern South Africa [26]. Regional circulation patterns show a weaker Angola Low (the source of the cloud bands) (Figure 9d), a stronger Botswana High, and hence more mid-level subsidence suppressing convection and cloud band formation (Figure 9c), and offshore moisture flux anomalies (Figure 9b) over northern KZN. The stronger Botswana High and weaker Angola Low in 2017/2018 are unlike the composite La Niña pattern derived for La Niña events during 1979–2021 that show a strong cyclonic anomaly in the lower and mid-troposphere (with widespread uplift over southern Africa) stretching right across southern Africa and the neighbouring subtropical and tropical ocean regions (Figure A5), which is also evident in the composite sea level pressure and surface wind anomalies [6]. Together with the cool SST anomalies south and east of South Africa, the north-westerly moisture flux anomalies over the southern Mozambique Channel/northern KZN coast (Figure 9b) imply a reduction in the onshore flow of moist marine air towards the eastern seaboard, and hence dry conditions. Thus, although the ENSO state indicated that 2017/2018 should have expected a wetter than average summer over eastern South Africa, regional SST and circulation patterns combined to produce very dry and relatively warm conditions.

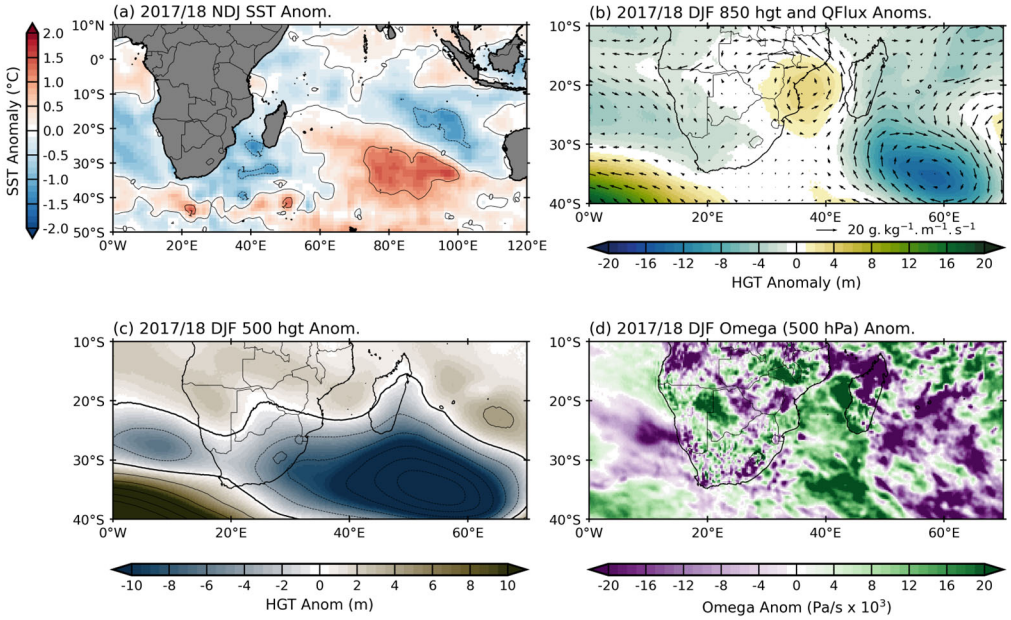

Figure 9. The 2017/2018 NDJ (**a**) SST anomalies (shaded; °C), (**b**) 850 geopotential height (shaded; m) and moisture flux (vectors; g kg^{-1} m^{-1} s^{-1}), (**c**) 500 hPa geopotential height (shaded; m), and (**d**) 500 hPa omega (shaded; Pa/s). The DJF mean (1979–2021 for ERA5 data and 1981–2021 NDJ for OISST data) of variables in panels a–c are provided in Figure A4.

3.3.3. Drought during Neutral Summer of 1981/1982

The 1981/1982 neutral summer is of particular interest because not only did it receive very low rainfall totals over all four regions but much of South Africa was also anomalously dry (Figure A2). In both KZN regions, this summer was the most severe of any in terms of rainfall metrics with only the 1982/1983 El Niño being comparable. During 1981/1982, regional SST anomalies were negative south of South Africa and in most of the southern West Indian Ocean (Figure 10a), unfavourable for summer rainfall over the country [26–29].

Furthermore, the Botswana High was shifted south-westward and stronger (Figure 10c), a pattern associated with widespread drought over subtropical southern Africa [30,31] since it suppresses convection and enhances subsidence. Most of subtropical southern Africa showed relative sinking at mid-levels in the troposphere (Figure 10d). As a result, the number of cloud bands occurring over South Africa during this summer was below average [20]. Low-level moisture flux anomalies (Figure 10b) show westerly anomalies along the south coast of South Africa in both seasons implying increased penetration of cooler, drier South Atlantic airmasses over the neighbouring land, consistent with drought [32].

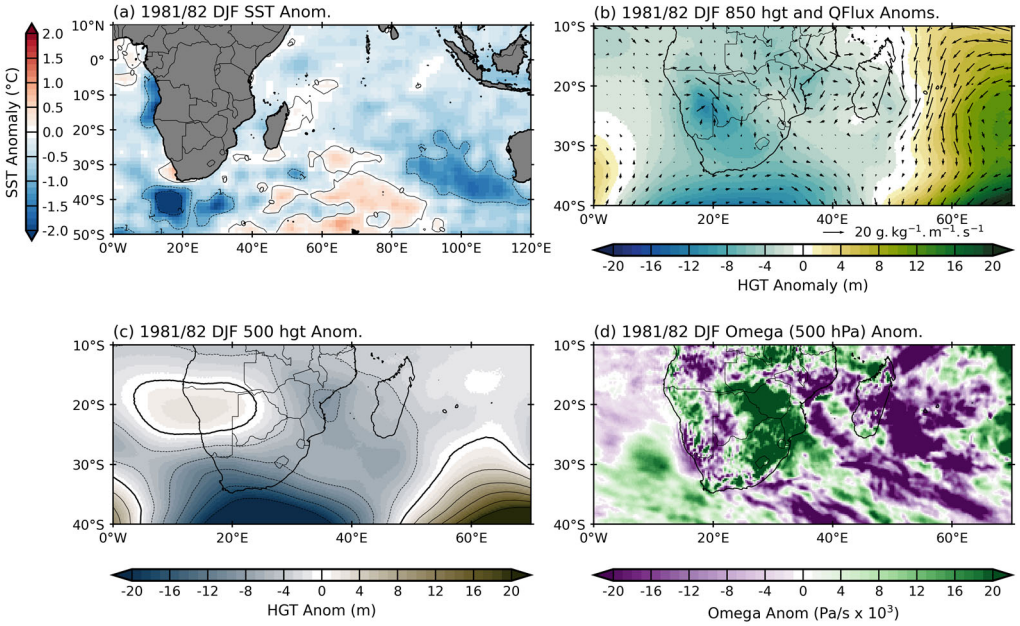

Figure 10. The 1981/1982 DJF (**a**) SST anomalies (shaded; °C), (**b**) 850 geopotential height (shaded; m) and moisture flux (vectors; g kg^{-1} m^{-1} s^{-1}), (**c**) 500 hPa geopotential height (shaded; m), and (**d**) 500 hPa omega (shaded; Pa/s). The DJF mean (1979–2021 for ERA5 data and 1981–2021 for OISST data) of variables in panels b–c are provided in Figure A4. Note that November 1981 data are not available in OISST, thus DJF data are shown here.

4. Discussion

Within the southern African climate and user group community, there is a general expectation that El Niño (La Niña) summers over most parts of subtropical southern Africa, including the eastern seaboard, are typically hot and dry (wet and cool). Indeed, summer rainfall totals do often more or less follow that expectation. This expectation is fanned by both official climate outlooks and the media who quite often tend to give an impression of an almost quasilinear relationship between the strength of an El Niño (La Niña) event and the severity of the expected summer drought (flood). However, caution is needed because there have been several prominent exceptions where this expectation has not been met, most obviously during the very strong 1997/1998 El Niño [7]. Furthermore, not enough attention is paid by either the forecasting community or the media to the way that the rainfall or temperature conditions vary during the particular ENSO summer. Although like rainfall totals, other metrics such as dry spell or hot day frequencies are fairly well correlated with indices such as Niño 3.4 over many parts of subtropical southern Africa (e.g., [3,15,16]), and therefore may have some predictability, such metrics do not seem to receive the attention they deserve. This relative lack of attention is unfortunate because these other metrics are often more important and impactful on the activities of user groups such as farmers, water resource managers, health workers, etc.

The eastern seaboard of subtropical southern Africa is a complex region meteorologically and is no exception to the tendency over southern Africa as a whole for the ENSO impact to be nonlinear and occasionally prone to widely diverging rainfall and temperature conditions from that forecast or expected during ENSO summers. In the north, the region is impacted by tropical lows and the occasional tropical cyclone [11] while some parts of the western basin of the Eastern Cape are semidesert and relatively close to the Mediterranean climate region further west. The warm Agulhas Current lies very close to the actual coastline along three of the four subregions analysed here, meaning that relatively moist and unstable marine air is present along much of this coast, helping facilitate the development of strong mesoscale convective systems quite often during the summer [33,34]. Near the border (~33°S) of the western and eastern drainage basins, the continental shelf widens, and the Agulhas Current starts to move further and further away from the coastline. Although all parts of the eastern seaboard receive summer rainfall from ridging anticyclones and tropical–extratropical cloud bands, the transition from relatively dry conditions in the southwest parts to a tropical climate in the far north, together with the large changes in topography, lead to a diverse range of ecosystems and agricultural activities along the eastern seaboard. Thus, in the far southwest, stone fruit, sheep, and some cattle are important in commercial farming whereas in KZN, sugar cane, dairy, tropical fruits, and forestry plantations dominate.

Parameter-space bubble plots of various rainfall and temperature metrics presented in this study provide a useful and relatively straightforward way in which to easily display the diversity of ENSO responses across the region and to rank the most adversely impacting events. These plots also show that many neutral summers in the region have in fact experienced similar or (in a few cases) worse impacts on the region than many ENSO events. Nonetheless, a few events such as 1982/1983 and 2015/2016 for El Niño and 1999/2000 for La Niña are clearly associated with the expected drought and flood conditions, respectively, across the region. While other ENSO events show a diversity in the strength of the expected impact, which is not related to the magnitude of the Niño 3.4 index, there are some exceptions that show completely the opposite of what the community associates with these events. The most obvious exceptions are the anomalously wet and cool 1987/1988 El Niño and the unusually dry and hot 2017/2018 La Niña. These summers also showed similar unexpected conditions over most of the summer rainfall region of South Africa as well as large parts of Mozambique, Zimbabwe, and Botswana. In these cases, it appears that regional forcing such as SST conditions in the southern West Indian Ocean and changes in the strength and location of the Botswana High (and thus in mid-level subsidence over the region) played important roles in the unexpected rainfall and temperature conditions experienced during 1987/1988 and 2017/2018.

5. Conclusions

Prominent deviations in rainfall and temperature characteristics during some ENSO summers away from the expected impacts pose challenges for seasonal forecasters and user groups, particularly farmers, as do the occasional neutral summers with very severe floods or droughts such as in 1981/1982. It is notable that the media as well as the forecasting community were already in April/May 2023 highlighting the possibility of a very strong El Niño developing during the remainder of 2023 and into 2024. The results presented in this study suggest that if this were to happen, it does not necessarily mean that DJF 2023/2024 will be very hot and dry over the eastern seaboard of subtropical southern Africa, or more broadly over the subcontinent. Although such conditions did occur during 1982/1983 and 2015/2016, they did not during the very strong 1997/1998 event, which remains as an important exception highlighting the need for caution in climate outlooks and briefings for farmers and other user groups. This study presented evidence that there is considerable diversity and nonlinearity in ENSO impact over eastern South Africa. Some of this nonlinearity in impacts may result from internal chaotic variability in the atmosphere, which poses further difficulties for long range forecasting and user groups.

Suitable designed climate model studies (e.g., [35] for nonlinear ENSO impacts over north-eastern Brazil) may shed further light on this issue. Finally, it is recommended that regional forecasting agencies consider providing specific information regarding dry spell frequencies and hot days to supplement their existing predictions of summer rainfall amounts (usually given as terciles). Both of these parameters appear to have a predictability based on their correlations with Niño 3.4 that are at least as high, if not higher than, rainfall amounts, and they are very relevant quantities for many farming and other user group activities.

Author Contributions: Conceptualization, R.C.B. and C.J.C.R.; methodology, R.C.B. and C.J.C.R.; software, R.C.B.; formal analysis, C.J.C.R. and R.C.B.; investigation, R.C.B.; resources, C.J.C.R.; data curation, R.C.B.; writing—original draft preparation, C.J.C.R.; writing—review and editing, R.C.B. and C.J.C.R.; visualization, R.C.B.; project administration, C.J.C.R.; funding acquisition, R.C.B. and C.J.C.R. All authors have read and agreed to the published version of the manuscript.

Funding: This research was partially funded by Royal Society (United Kingdom) and African Academy of Sciences, through the FLAIR Programme, grant number FLR\R1\201615.

Institutional Review Board Statement: Not applicable.

Informed Consent Statement: Not applicable.

Data Availability Statement: The ERA5 data used were downloaded from the Copernicus Climate Change Service (C3S) Climate Data Store (accessed 12 July 2022). ERSSTv5 data used in Figure 3 can be obtained from https://www.ncei.noaa.gov/products/extended-reconstructed-sst (accessed 22 October 2022).

Acknowledgments: R.C.B. acknowledges support of the FLAIR programme, a partnership between the African Academy of Sciences and the Royal Society funded by the UK Government's Global Challenges Research Fund.

Conflicts of Interest: The authors declare no conflict of interest.

Appendix A

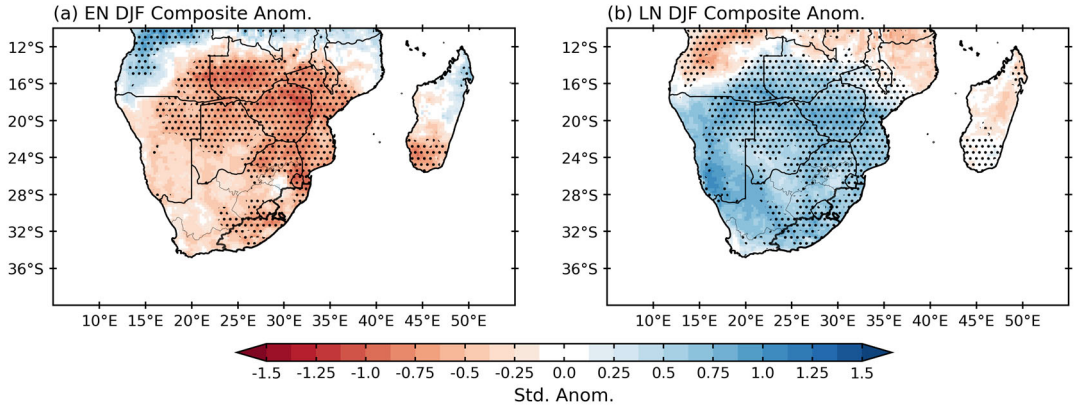

Figure A1. Mean DJF composite of standardized rainfall anomaly across southern Africa during (**a**) El Niño and (**b**) La Niña events. Based on Figures 4–7 and the ±0.75 °C threshold used in the study, there are 9 El Niño events and 12 La Niña events over the 1979–2021 period that are used to create the composite. Stippling in the figure denotes values that are statistically significant at the 95% level based on a two-tailed nonparametric Monte Carlo bootstrap significance test. Given the smaller size of the panels, only the location of the Eastern Cape and KZN provinces in South Africa are highlighted as the two black polygon outlines.

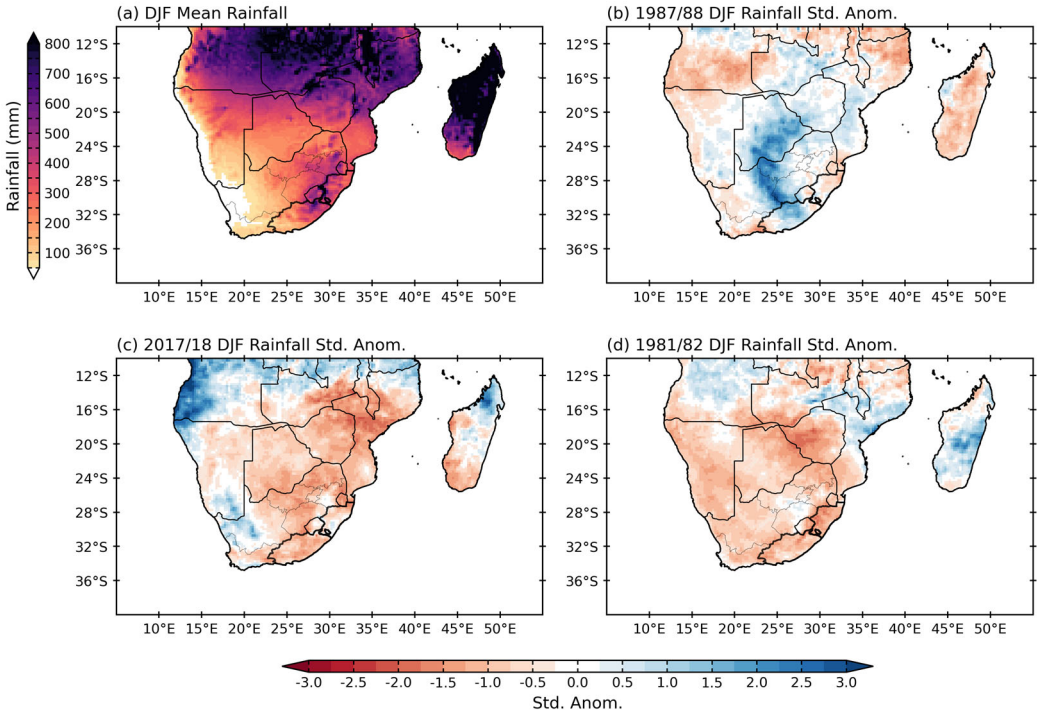

Figure A2. (**a**) Mean DJF rainfall (shaded; mm) across southern Africa. The DJF standardized rainfall anomalies for (**b**) 1987/1988, (**c**) 2017/2018, and (**d**) 1981/1982. The location of the Eastern Cape and KZN provinces in South Africa are highlighted by the two black polygon outlines.

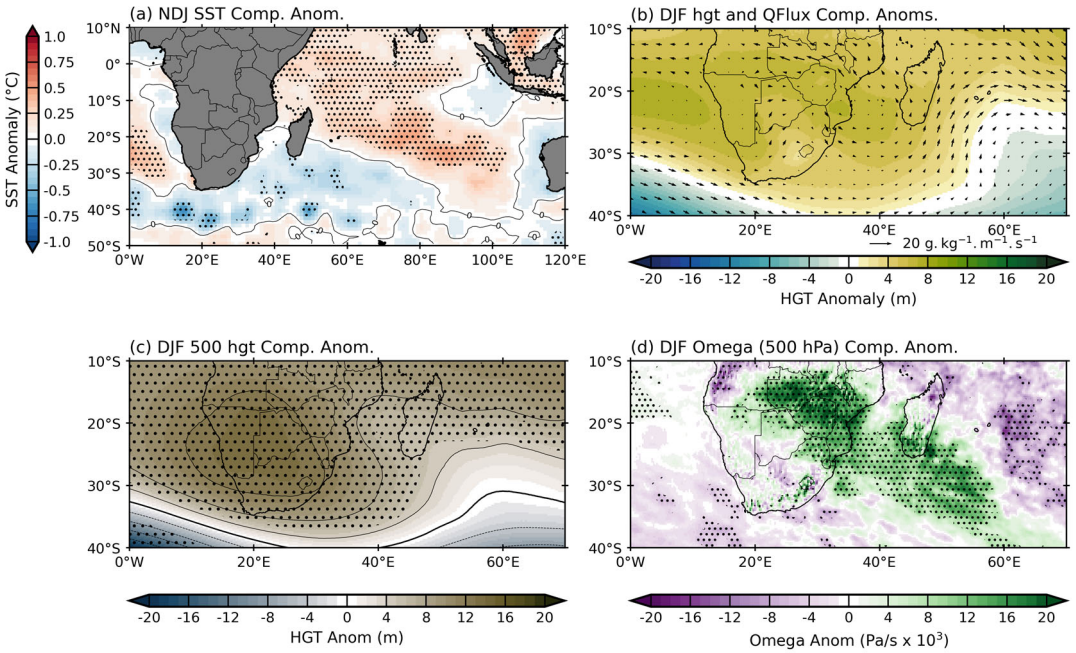

Figure A3. The El Niño composite mean of (**a**) NDJ SST anomalies, (**b**) DJF 850 geopotential height and moisture flux anomalies, (**c**) DJF 500 hPa geopotential height, and (**d**) DJF 500 hPa omega. Based on Figures 4–7, there are nine El Niño events that are used to create the composite. Stippling in the figure denotes values that are statistically significant at the 95% level based on a two-tailed nonparametric Monte Carlo bootstrap significance test. For ease of viewing the vectors in panel (**b**), no stippling is shown.

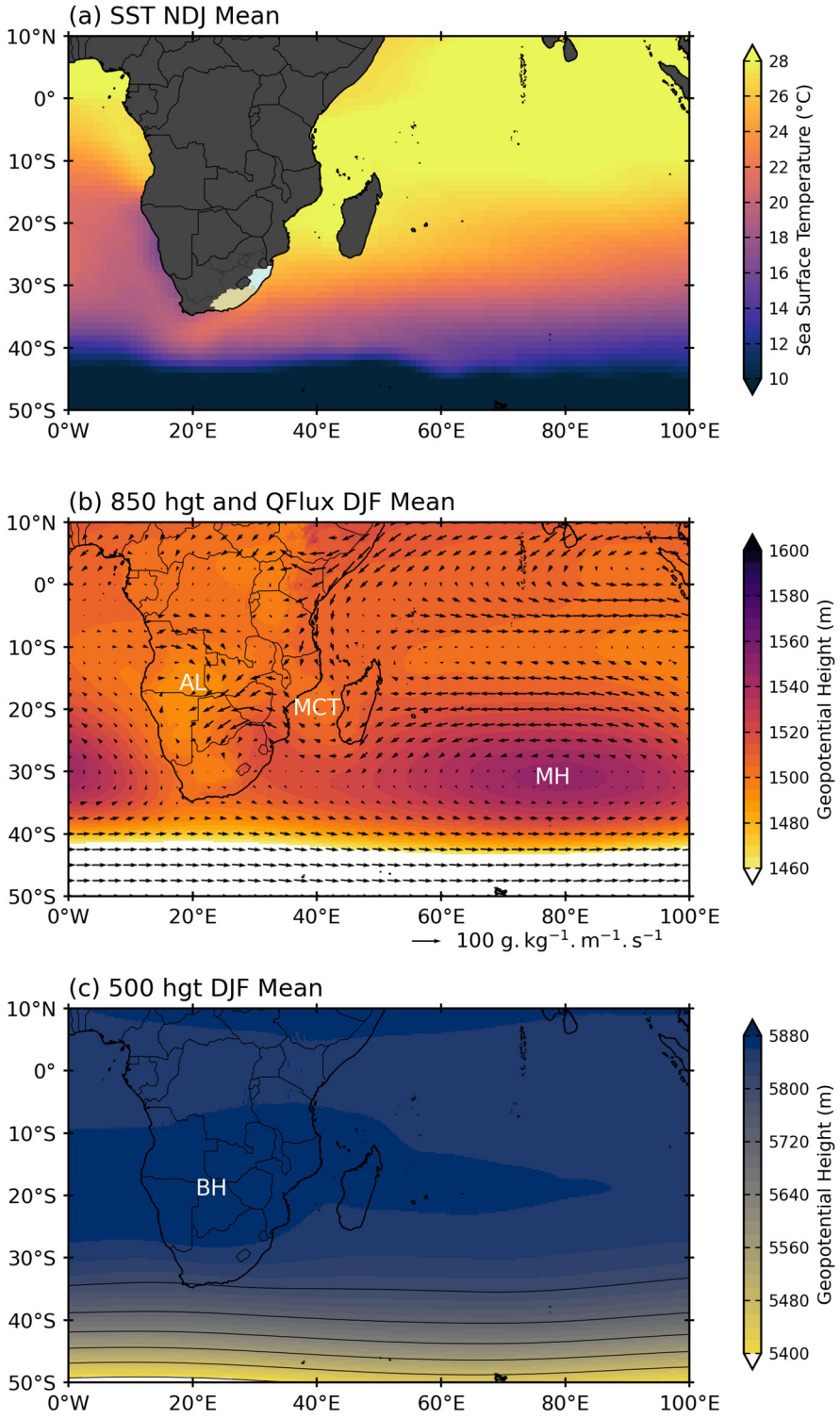

Figure A4. (**a**) The mean SST (shaded; °C) around southern Africa during NDJ from OISST data; (**b**) the mean DJF 850 hPa geopotential height (shaded; m) and moisture flux (vector; g·kg^{-1}·m^{-1}·s^{-1}); (**c**) the mean DJF 500 geopotential height (shaded; m). The location of the Eastern Cape and KZN provinces in South Africa are highlighted by the two polygons in panel (**a**). The DJF mean locations of the Mascarene High (MH), Mozambique Channel Trough (MCT), and Angola Low (AL) are provided in panel (**b**), while the mean position of the Botswana High (BH) is highlighted in panel (**c**).

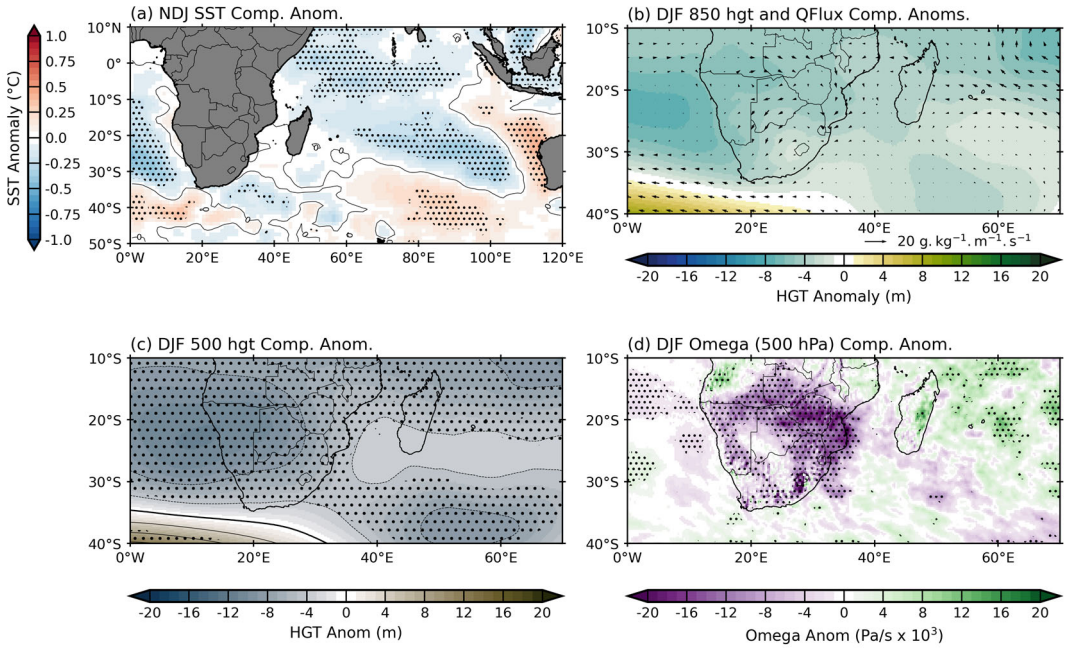

Figure A5. The La Niña composite mean of (**a**) NDJ SST anomalies, (**b**) DJF 850 geopotential height and moisture flux anomalies, (**c**) DJF 500 hPa geopotential height, and (**d**) DJF 500 hPa omega. Based on Figures 4–7, there are 12 La Niña events that are used to create the composite. Stippling in the figure denotes values that are statistically significant at the 95% level based on a two-tailed nonparametric Monte Carlo bootstrap significance test. For ease of viewing the vectors in panel (**b**), no stippling is shown.

References

1. Mahlalela, P.; Blamey, R.; Hart, N.; Reason, C. Drought in the Eastern Cape region of South Africa and trends in rainfall characteristics. *Clim. Dyn.* **2020**, *55*, 2743–2759. [CrossRef] [PubMed]
2. Thoithi, W.; Blamey, R.C.; Reason, C.J.C. April 2022 Floods over East Coast South Africa: Interactions between a Mesoscale Convective System and a Coastal Meso-Low. *Atmosphere* **2023**, *14*, 78. [CrossRef]
3. Thoithi, W.; Blamey, R.C.; Reason, C.J.C. Dry spells, wet days, and their trends across Southern Africa during the summer rainy season. *Geophys. Res. Lett.* **2021**, *48*, e2020GL091041. [CrossRef]
4. Ropelewski, C.F.; Halpert, M.S. Global and regional precipitation patterns associated with El Niño/southern oscillation. *Mon. Weather Rev.* **1987**, *115*, 1606–1626. [CrossRef]
5. Lindesay, J. South African rainfall, the Southern Oscillation and a Southern Hemisphere semi-annual cycle. *J. Climatol.* **1988**, *8*, 17–30. [CrossRef]
6. Reason, C.J.C.; Allan, R.J.; Lindesay, J.A.; Ansell, T.J. ENSO and climatic signals across the Indian Ocean basin in the global context: Part I. Interannual composite patterns. *Int. J. Climatol.* **2000**, *20*, 1285–1327. [CrossRef]
7. Reason, C.J.C.; Jagadheesha, D. A model investigation of recent ENSO impacts over southern Africa. *Meteor. Atmos. Phys.* **2005**, *89*, 181–205. [CrossRef]
8. Lyon, B.; Mason, S.J. The 1997–98 summer rainfall season in southern Africa. Part I: Observations. *J. Clim.* **2007**, *20*, 5134–5148. [CrossRef]
9. Blamey, R.C.; Kolusu, S.R.; Mahlalela, P.; Todd, M.C.; Reason, C.J.C. The role of regional circulation features in regulating El Niño climate impacts over southern Africa: A comparison of the 2015/2016 drought with previous events. *Int. J. Climatol.* **2018**, *38*, 4276–4295. [CrossRef]
10. Driver, P.; Abiodun, B.; Reason, C.J.C. Modelling the precipitation response over southern Africa to the 2009–2010 El Niño using a stretched grid global atmospheric model. *Clim. Dyn.* **2019**, *52*, 3929–3949. [CrossRef]
11. Mpungose, N.; Thoithi, W.; Blamey, R.C.; Reason, C.J.C. Extreme rainfall events in southeastern Africa during the summer. *Theor. Appl. Climatol.* **2022**, *150*, 185–201. [CrossRef]
12. Hersbach, H.; Bell, B.; Berrisford, P.; Hirahara, S.; Horányi, A.; Muñoz-Sabater, J.; Nicolas, J.; Peubey, C.; Radu, R.; Schepers, D.; et al. The ERA5 global reanalysis. *Q. J. R. Meteorol. Soc.* **2020**, *146*, 1999–2049. [CrossRef]
13. Huang, B.; Thorne, P.W.; Banzon, V.F.; Boyer, T.; Chepurin, G.; Lawrimore, J.H.; Menne, M.J.; Smith, T.M.; Vose, R.S.; Zhang, H.-M. Extended Reconstructed Sea Surface Temperature version 5 (ERSSTv5), Upgrades, validations, and intercomparisons. *J. Clim.* **2017**, *30*, 8179–8205. [CrossRef]

14. Reynolds, R.W.; Smith, T.M.; Liu, C.; Chelton, D.B.; Casey, K.S.; Schlax, M.G. Daily high-resolution-blended analyses for sea surface temperature. *J. Clim.* **2007**, *20*, 5473–5496. [CrossRef]
15. Usman, M.T.; Reason, C.J.C. Dry spell frequencies and their variability over southern Africa. *Clim. Res.* **2004**, *26*, 199–211. [CrossRef]
16. Reason, C.J.C.; Hachigonta, S.; Phaladi, R.F. Interannual variability in rainy season characteristics over the Limpopo region of southern Africa. *Int. J. Climatol.* **2005**, *25*, 1835–1853. [CrossRef]
17. Weldon, D.; Reason, C.J.C. Variability of rainfall characteristics over the South Coast region of South Africa. *Theor. Appl. Climatol.* **2014**, *115*, 177–185. [CrossRef]
18. Engelbrecht, C.J.; Landman, W.A.; Engelbrecht, F.A.; Malherbe, J. A synoptic decomposition of rainfall over the Cape south coast of South Africa. *Clim. Dyn.* **2015**, *44*, 2589–2607. [CrossRef]
19. Ndarana, T.; Mpati, S.; Bopape, M.-J.; Engelbrecht, F.; Chikoore, H. The flow and moisture fluxes associated with ridging South Atlantic Ocean anticyclones during the subtropical southern African summer. *Int. J. Climatol.* **2020**, *41*, E1000–E1017. [CrossRef]
20. Hart, N.C.; Reason, C.J.C.; Fauchereau, N. Cloud bands over Southern Africa: Seasonality, contribution to rainfall variability and modulation by the MJO. *Clim. Dyn.* **2013**, *41*, 1199–1212. [CrossRef]
21. Beraki, A.F.; Landman, W.A.; DeWitt, D. On the comparison between seasonal predictive skill of global circulation models: Coupled versus uncoupled. *J. Geophys. Res. Atmos.* **2015**, *120*, 11151–11172. [CrossRef]
22. Ratnam, J.V.; Behera, S.K.; Masumoto, Y.; Yamagata, T. Remote effects of El Niño and Modoki events on the austral summer precipitation of Southern Africa. *J. Clim.* **2014**, *27*, 3802–3815. [CrossRef]
23. Behera, S.K.; Yamagata, T. Subtropical SST dipole events in the southern Indian Ocean. *Geophys. Res. Lett.* **2001**, *28*, 327–330. [CrossRef]
24. Reason, C.J.C. Subtropical Indian Ocean SST dipole events and southern African rainfall. *Geophys. Res. Lett.* **2001**, *28*, 2225–2227. [CrossRef]
25. Reason, C.J.C. Sensitivity of the Southern African circulation to dipole Sea-Surface Temperature patterns in the South Indian Ocean. *Int. J. Climatol.* **2002**, *22*, 377–393. [CrossRef]
26. Reason, C.J.C.; Mulenga, H. Relationships between South African rainfall and SST anomalies in the southwest Indian Ocean. *Int. J. Climatol.* **1999**, *19*, 1651–1673. [CrossRef]
27. Walker, N. Links between South African summer rainfall and temperature variability of the Agulhas and Benguela Current systems. *J. Geophys. Res. Ocean.* **1990**, *95*, 3297–3319. [CrossRef]
28. Mason, S. Sea-surface temperature-South African rainfall associations, 1910–1989. *Int. J. Climatol.* **1995**, *15*, 119–135. [CrossRef]
29. Reason, C.J.C. Interannual warm and cool events in the subtropical / mid-latitude South Indian Ocean region. *Geophys. Res. Lett.* **1999**, *26*, 215–218. [CrossRef]
30. Reason, C.J.C. The Bolivian, Botswana and Bilybara Highs and Southern Hemisphere drought/floods. *Geophys. Res. Lett.* **2016**, *43*, 1280–1286. [CrossRef]
31. Driver, P.; Reason, C.J.C. Variability in the Botswana High and its relationships with rainfall and temperature characteristics over southern Africa. *Int. J. Climatol.* **2017**, *37*, 570–581. [CrossRef]
32. Mulenga, H.M.; Rouault, M.; Reason, C.J.C. Dry summers over northeastern South Africa and associated circulation anomalies. *Clim. Res.* **2003**, *25*, 29–41.
33. Blamey, R.C.; Reason, C.J.C. Mesoscale convective complexes over southern Africa. *J. Clim.* **2012**, *25*, 753–766. [CrossRef]
34. Morake, D.M.; Blamey, R.C.; Reason, C.J.C. Long-lived mesoscale convective systems over eastern South Africa. *J. Clim.* **2021**, *34*, 6421–6439. [CrossRef]
35. Kay, G.; Dunstone, N.J.; Smith, D.M.; Betts, R.A.; Cunningham, C.; Scaife, A.A. Assessing the chance of unprecedented dry conditions over North Brazil during El Niño events. *Environ. Res. Lett.* **2022**, *17*, 064016. [CrossRef]